PAPER

CrossMark
click for updates

A DFT-based comparative equilibrium study of thermal dehydration and hydrolysis of $CaCl_2$ hydrates and $MgCl_2$ hydrates for seasonal heat storage

Amar Deep Pathak,* Silvia Nedea, Herbert Zondag, Camilo Rindt and David Smeulders

Salt hydrates store solar energy in chemical form *via* a reversible dehydration–hydration reaction. However, as a side reaction to dehydration, hydrolysis (HCl formation) may occur in chloride based salt hydrates (specially in $MgCl_2$ hydrates), affecting the durability of the storage system. The mixture of $CaCl_2$ and $MgCl_2$ hydrates has been shown experimentally to have exceptional cycle stability and improved kinetics. However, the optimal operating conditions for the mixture are unknown. To understand the appropriate balance between dehydration and hydrolysis kinetics in the mixtures, it is essential to gain in-depth insight into the mixture components. We present a GGA-DFT level study to investigate the various gaseous structures of $CaCl_2$ hydrates and to understand the relative stability of their conformers. The hydration strength and relative stability of conformers are dominated by electrostatic interactions. A wide network of intramolecular homonuclear and heteronuclear hydrogen bonds is observed in $CaCl_2$ hydrates. Equilibrium product concentrations are obtained during dehydration and hydrolysis reactions under various temperature and pressure conditions. The trend of the dehydration curve with temperature in $CaCl_2$ hydrates is similar to the experiments. Comparing these results to those of $MgCl_2$ hydrates, we find that $CaCl_2$ hydrates are more resistant towards hydrolysis in the temperature range of 273–800 K. Specifically, the present study reveals that the onset temperatures of HCl formation, a crucial design parameter for $MgCl_2$ hydrates, are lower than for $CaCl_2$ hydrates except for the mono-hydrate.

1 Introduction

Solar thermal energy can be stored in three forms: sensible heat, latent heat, and in thermochemical form. In a thermochemical storage system, energy is stored by bond breaking and reformation in a reversible reaction.[1] Compared to sensible or latent heat, the energy storage density is higher in thermochemical form.[2] This explains the enormous interest in thermochemical materials (TCMs) for seasonal heat storage applications.[3] TCMs offer compact solar energy storage suitable for household applications. TCMs are widely available and inexpensive, and therefore appear to be an attractive material for seasonal heat storage. The cost of TCM is 30% of the total investment in the thermochemical heat storage system.[3] Thus, the selection of TCMs is a key aspect in designing the heat storage system.

Salt hydrates are one class of TCMs. Upon charging, these materials absorb solar energy and disintegrate into a lower hydrated or anhydrous form. Upon discharging, these dried salt

Energy Technology, P. O. Box 513 5600 MB Eindhoven, The Netherlands.
E-mail: a.d.pathak@tue.nl

hydrates recombine with H_2O, forming hydrates while dissipating energy.

$$\text{Salt} \cdot n\text{H}_2\text{O} \rightleftharpoons \text{Salt} + n\text{H}_2\text{O} \qquad (1)$$
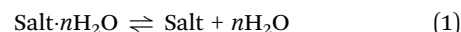
The forward reaction is endothermic while the backward reaction is exothermic. The major challenge in selection of these salt hydrates is to find materials with high storage capacity, cycle stability and fast kinetics. $MgSO_4$ hydrates have a high storage capacity (2–3 GJ m^{-3}). However, $MgSO_4$ hydrates have sluggish hydration kinetics due to the presence of strong hydrogen bonds (H-bonds).[4] Chloride based salt hydrates ($MgCl_2 \cdot n\text{H}_2\text{O}$, $CaCl_2 \cdot n\text{H}_2\text{O}$, n = 0, 1, 2, 4, and 6) are also promising TCMs for seasonal heat storage. They have high storage capacity (2–3 GJ m^{-3}). However, hydrolysis is reported for chloride based salt hydrates. This is an irreversible endothermic reaction which competes with dehydration reaction, according to

$$\text{MCl}_2 \cdot n\text{H}_2\text{O} \rightarrow \text{MOHCl} + (n - 1)\text{H}_2\text{O} + \text{HCl (M = Mg/Ca)} \qquad (2)$$
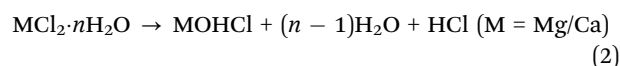
$MgCl_2$ hydrates have faster kinetics but also have the problem of hydrolysis as a side reaction.[5] Hydrolysis affects the cycle

This journal is © the Owner Societies 2016

Phys. Chem. Chem. Phys., 2016, **18**, 10059–10069 | 10059

stability of the storage system and generates HCl gas, which is harmful and corrosive. This poses a challenge for the application of MgCl$_2$ hydrate as a TCM.

Hydrolysis can be avoided in TCMs by mixing with other halides.[6] Rammelberg et al.[7] examined the performance of various salt mixtures. They observed that the mixture of CaCl$_2$ hydrates and MgCl$_2$ hydrates shows good cycle stability and improved kinetics compared to MgCl$_2$ and CaCl$_2$ hydrates alone. They have not described the chemical explanation for this extra stability. To assess the performance of the mixture of CaCl$_2$ hydrates and MgCl$_2$ hydrates, it is essential to investigate the dehydration and hydrolysis behavior of CaCl$_2$ hydrates and compare these to MgCl$_2$ hydrates.

CaCl$_2$ hydrate has been used as a TCM.[8–11] It has a very high crystalline energy storage density (2.82 GJ m^{-3}), is readily available, inflammable and has high temperature lift during hydration.[3,8,12] CaCl$_2$ hydrates are also used in mobile storage of industrial waste.[13] In domestic heat storage systems, TCMs are used in the temperature range of 300–500 K while in mobile storage of industrial heat, a much higher temperature range is used. Thus, it is important to investigate the equilibrium products of dehydration and hydrolysis reactions of CaCl$_2$ hydrates over a wide temperature range. Next to the kinetics of dehydration/hydrolysis, the onset temperature of HCl formation in chloride based salt hydrates is a crucial parameter in designing heat storage systems.

Rammelberg et al.[10] and Zondag et al.[9] examined the kinetics of dehydration of CaCl$_2$ hydrates using Thermogravimetric analysis (TGA) and did not observe hydrolysis. Fraissler et al.[14] observed that the formation of HCl gas from the hydrolysis of CaCl$_2$ occurs in a certain temperature range (683–1013 K). In these temperature regimes the preference of hydrolysis over dehydration reaction is ambiguous from experiments.

Computational models can be successfully used to investigate the in-depth behavior of salt hydrates in different temperature regimes.[4,15–18] The hydration of Ca^{2+} ions has been successfully investigated using Density Functional Theory (DFT),[19,20] molecular dynamics simulations[18,21] and validated by experiments.[22,23] Iype et al.[4] characterized the H-bonds present in MgSO$_4$ hydrates using DFT calculations. They observed that strong H-bonds affect the hydration kinetics of MgSO$_4$ hydrates. Smeets et al.[15] computationally investigated the dehydration and hydrolysis reactions for MgCl$_2$ hydrates. They have reported the equilibrium curves for dehydration/hydrolysis of MgCl$_2$ hydrates. We have explored the relative stability of various conformers of CaCl$_2$ hydrates, ideal operating conditions of CaCl$_2$ hydrates and compared them with MgCl$_2$ hydrates.[15] Nevertheless, to the best of our knowledge, currently no computational studies exist on the hydrolysis reaction of CaCl$_2$ hydrates, the onset temperature of HCl formation and their comparison with MgCl$_2$ hydrates. The system level complexity of salt hydrate mixtures like grain boundaries, grain sizes and their effect on the reaction kinetics could be addressed by multiscale integration of DFT results to the system level.[24]

In the present study, we would like to understand by means of DFT calculations, the temperature and pressure conditions under which hydrolysis precedes over dehydration. First we examine the molecular structure and vibrational frequencies of CaCl$_2$ hydrates and their conformers. We investigate the strength of H-bonds present in CaCl$_2$ hydrates, since strong H-bonds can result in sluggish hydration kinetics. We characterize the H-bonds using the Bond Valence (BV) sum rule. The BV sum rule is frequently used to correlate the structural properties of H-bonds and crystal structure determination.[4,25,26] The enthalpy of the dehydration and hydrolysis reactions of CaCl$_2$ hydrates is obtained from DFT calculations and compared to MgCl$_2$ hydrates. The change in Gibbs free energy for dehydration and hydrolysis of all hydrates is obtained, followed by the equilibrium product concentration. The equilibrium properties obtained from the present DFT calculations can be used to calculate safety limits for thermal degradation of CaCl$_2$ hydrates. These safety limits are compared with MgCl$_2$ hydrates.

2 Computational model and validation

2.1 Density functional theory calculations

The molecular structures of various CaCl$_2$ hydrates, their conformers, HCl, H$_2$O, and CaOHCl are fully optimized in DFT using the Perdew–Wang exchange and correlation functional (PW91) under generalized gradient approximation (GGA)[27] implemented in the Amsterdam Density Functional (ADF) program[28] with the double-polarized triple-ζ basis set. A spin restricted Kohn–Sham method is used thus keeping the maximum integration accuracy. DFT-GGA has been used to study the salt hydrates like CaCl$_2$, MgCl$_2$, MgSO$_4$.[4,15–17] Iype et al.[4] showed the applicability of GGA-DFT to study the H-bonds present in hydrates of MgSO$_4$.

2.2 Model validation

To validate the applicability of GGA-DFT using the PW91 functional, we have examined the binding enthalpy, Ca–O coordination length and vibrational frequency of [Ca(H$_2$O)$_6$]$^{2+}$ ions. The successive binding enthalpy of hexahydrated Ca^{2+} ions $\left(\Delta H^{\circ}_{6,5}\right)$ is defined as

$$\Delta H^{\circ}_{6,5} = H^{\circ}_{\text{Ca(H}_2\text{O)}_6^{2+}} - H^{\circ}_{\text{Ca(H}_2\text{O)}_5^{2+}} - H^{\circ}_{\text{H}_2\text{O}} \qquad (3)$$

The optimized structure of [Ca(H$_2$O)$_6$]$^{2+}$ is shown in Fig. 1. We estimated the successive binding enthalpy of [Ca(H$_2$O)$_6$]$^{2+}$ ions from GGA-DFT to be 26.26 kcal mol^{-1}, which is in close agreement with previous DFT calculations (26.37 kcal mol^{-1})[20] and experimental results (25.3 kcal mol^{-1}).[22]

In the present DFT study, the average coordination length of Ca–O in the first hydration shell of Ca^{2+} is 2.39 Å, which is in excellent agreement with past DFT results (2.37 Å),[19] high order Car–Parrinello molecular dynamics results (2.41 Å)[21] and experimental results (2.39 Å, XRD).[29] Furthermore, we have calculated the vibrational frequencies of [Ca(H$_2$O)$_6$]$^{2+}$. The IR peak position obtained from present calculations are in close agreement with Lei and Pan[20] as shown in Fig. 2.

10060 | *Phys. Chem. Chem. Phys.*, 2016, **18**, 10059–10069

This journal is © the Owner Societies 2016
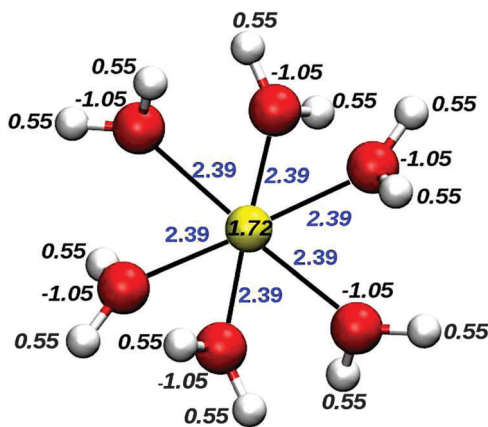
Fig. 1 Optimized structure of hydrated Ca^{2+} ions ($[Ca(H_2O)_6]^{2+}$). Bader charges (black, italic) and Ca–O coordination lengths (in Å, blue) are shown. Color scheme: Ca = yellow, O = red, and H = white.
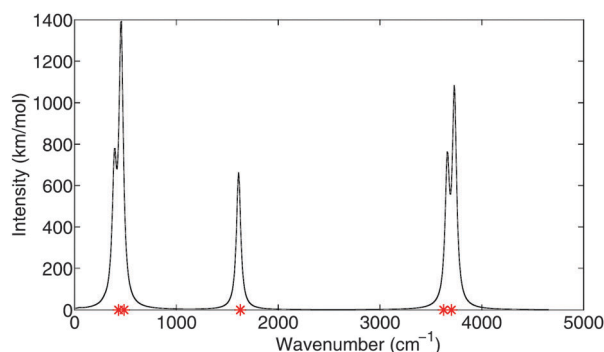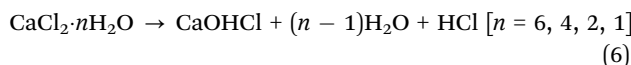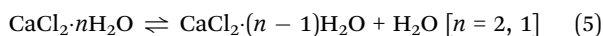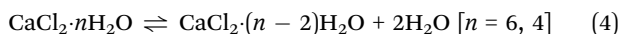

Fig. 2 The calculated IR spectra of the ground state structure of $[Ca(H_2O)_6]^{2+}$. The represents the IR peak position of $[Ca(H_2O)_6]^{2+}$ ions, as reported by Lei and Pan.[20]

2.3 Methodology

The harmonic frequencies of each optimized geometry are calculated to quantify the vibrational contribution of energy and entropy. The information of vibrational spectra, ground state geometry and Gibbs free energy (G) of all reactants and products are essential to calculate ΔG of dehydration and hydrolysis reaction.[30] In the present study, we are interested in the following dehydration and hydrolysis reactions of $CaCl_2$ hydrates:

$$CaCl_2 \cdot nH_2O \rightleftharpoons CaCl_2 \cdot (n-2)H_2O + 2H_2O \ [n = 6, 4] \quad (4)$$

$$CaCl_2 \cdot nH_2O \rightleftharpoons CaCl_2 \cdot (n-1)H_2O + H_2O \ [n = 2, 1] \quad (5)$$

$$CaCl_2 \cdot nH_2O \rightarrow CaOHCl + (n-1)H_2O + HCl \ [n = 6, 4, 2, 1] \quad (6)$$

The change in the Gibbs free energy of above reactions is expressed as

$$\Delta G = \sum G_{product} - \sum G_{reactant} \quad (7)$$

The equilibrium product concentration of dehydration and hydrolysis reactions can be obtained by equating ΔG to zero. For the ΔG calculation, the physical state of each reactant and product is important. Experimentally, $CaCl_2$ hydrates remain in the solid phase, and H_2O and HCl exist in the gaseous phase. However, the precise frequency calculation, subsequently the Gibbs free energy of solid $CaCl_2$ hydrates over a wide temperature range, is computationally challenging. The periodic unit cell of these $CaCl_2$ hydrates contains 36, 90, and 21 atoms for di, tetra, and hexahydrates respectively.[31–35] Due to the large size of Ca and Cl atoms and a large number of atoms in unit cell, the Gibbs free energy calculation of the crystalline phase is expensive. Weck et al.[36] obtained the Gibbs free energy of solid $MgCl_2$ hydrates under quasi-harmonic approximation (QHA) from GGA-DFT calculations. The Gibbs free energy of the crystalline phase obtained from QHA may breakdown at higher temperature. Despite the fact that these calculations were done for another solid salt hydrates ($MgCl_2 \cdot nH_2O$), it should also be valid for $CaCl_2 \cdot nH_2O$. Nevertheless, the solid reactant and product do not always remain in the crystalline phase and hydrolysis is expected to occur in the liquid phase.[15] Thus for a solid–gas reaction, ΔG can be estimated by Gibbs free energy of the gaseous phase (G_{gas}). The equilibrium product concentration obtained under gas assumption will be considered as the safety limit of these reactions in seasonal heat storage systems.

In this paper, the ΔG in dehydration and hydrolysis reactions is computed under ideal poly-atomic gas assumption[30] assuming each reactant and product to be in the gaseous state. Gibbs free energy of a gaseous molecule at given temperature T and absolute pressure p can be given as

$$G(T,p) = U + pV - TS \quad (8)$$

The partition function of an ideal poly-atomic gas can be expressed as[30]

$$q = q_{trans}q_{rot}q_{vib}q_{elec} \quad (9)$$

where q is the partition function and q_{trans}, q_{rot}, q_{vib}, and q_{elec} are their translational, rotational, and electronic contributions.

Internal energy U of poly-atomic gas can be expressed as

$$U(T,p) = 3RT + R\sum_{j=1}^{3N-6}\left(\frac{\Theta_{vib,j}}{2} + \frac{\Theta_{vib,j}}{e^{-\Theta_{vib,j}/T} - 1}\right) + U_{gr} \quad (10)$$

where R is the gas constant, $\Theta_{vib,j}$ is vibrational temperature ($h\nu/k_b$) of the jth atom, ν is the frequency of the vibrational mode, h is Planck's constant, k_b is the Boltzmann constant and U_{gr} is the ground state energy of the molecule.

The entropy (S) of poly-atomic gas can be expressed as

$$\begin{aligned} S(T,p) = {} & R\left[\ln\left(\frac{k_bT}{p}\left(\frac{2\pi Mk_bT}{h^2}\right)^{3/2}\right) + \frac{3}{2}\right] \\ & + R\sum_{j=1}^{3N-6}\left(\frac{\Theta_{vib,j}/T}{e^{-\Theta_{vib,j}/T} - 1}\right) \\ & + R\sum_{j=1}^{3N-6}\left[\ln\left(1 - e^{-\Theta_{vib,j}/T}\right)\right] + S_{rot}, \end{aligned} \quad (11)$$

where M is the total atomic mass and S_{rot} is the rotational contribution of entropy and can be expressed for the asymmetrical top molecule as[30]

$$S_{rot} = R\left[\ln\left(\frac{\sqrt{\pi I_a I_b I_c}}{\sigma}\left(\frac{8\pi^2 k_b T}{h^2}\right)^{3/2}\right) + \frac{3}{2}\right] \quad (12)$$

where I_a, I_b, and I_c are three principle moments of inertia and σ is the symmetry number of the molecule, which is the number of rotational modes of the molecule. From the optimized geometry of the molecule, we have obtained the U_{gr}, principle moment of inertia and frequency of its vibrational mode. Eqn (7) and (8) are used to calculate ΔG of a particular dehydration or hydrolysis reaction at given T and p.

The H-bonds of CaC_2 hydrates are analyzed in the gaseous phase. This is a valid analysis as the locus of H-bond parameters can be generalized irrespective of the system being in a condensed phase or the gaseous phase.[4] The presence of H-bonds is identified by the non-bonded $X\cdots H$ ($X = Cl$ and O) distance. When the non-bonded distance between O and H varies from 1.5 Å to 2.0 Å, we classify these H-bonds as OHO homonuclear type H-bonds, which is consistent with Iype et al.[4] Similarly, when the non-bonded distance between Cl and H varies from 1.9 Å to 2.5 Å, we classify these H-bonds as a OHCl heteronuclear type H-bond. Bader charges on various atoms in the molecule are calculated to understand the charge distribution. We compared the charge distribution in all hydrates to observe charge transfer, the effect of Coulombic interactions on their stability and enthalpy of dehydration.

3 Results and discussions

The gaseous structures of $CaCl_2$ hydrates are investigated to understand the H-bond network, relative stability of conformers and enthalpy change in the hydrolysis and dehydration reactions. The optimized structures are used to obtain vibrational frequencies, and their entropic and energy contribution from DFT calculations. In this section, we present the optimized structures of $CaCl_2$ hydrates and their conformers.

3.1 Molecular structures of $CaCl_2$ hydrates and their conformers

3.1.1 Anhydrous $CaCl_2$, CaOHCl, and $CaCl_2\cdot H_2O$.
The gaseous anhydrous $CaCl_2$ molecule is optimized with many initial configurations and all converged into the final $CaCl_2$ structure as shown in Fig. 3a. The structure of $CaCl_2$ is linear with the Ca–Cl bond length being 2.45 Å. The structural properties of $CaCl_2$ are in agreement with the experimental crystalline structures of $CaCl_2$.[37] The optimized structure of CaOHCl is shown in Fig. 3b. CaOHCl is a non-linear molecule with Ca–Cl and Ca–O bond lengths of 2.49 Å and 1.99 Å. The optimized structure of $CaCl_2\cdot H_2O$ is shown in Fig. 3c. The Ca–O coordination length is 2.33 Å. The hydrated H_2O forms a H-bond with one of the Cl atoms of $CaCl_2$ and stretched the Ca–Cl distance by 0.08 Å. The Bader charge of a Cl atom participating in H-bonding differs by 0.02 to that of a Cl atom not participating.
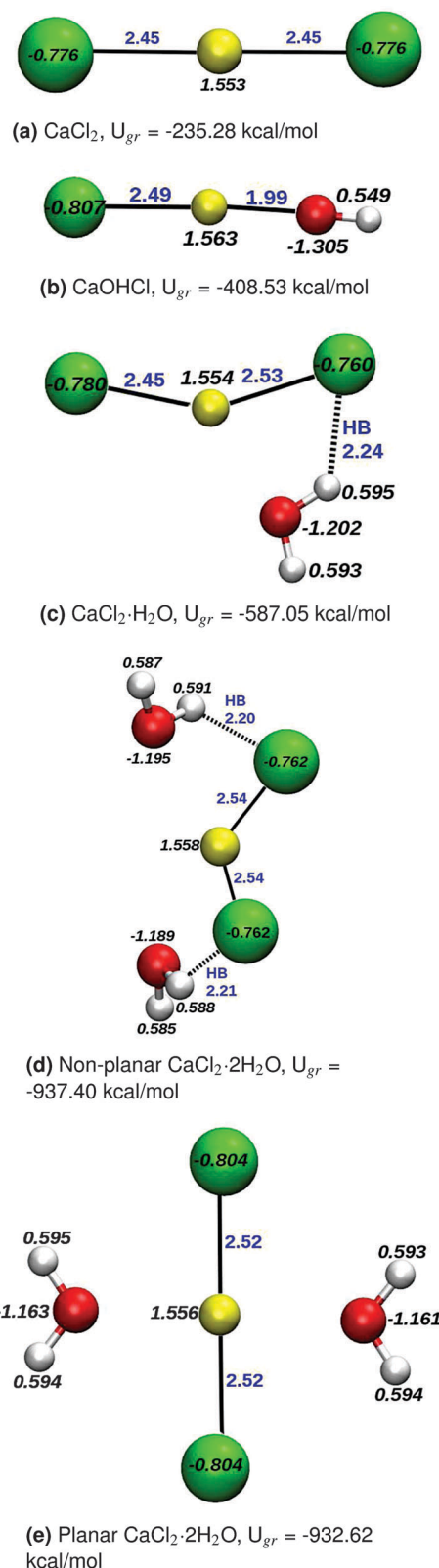

Fig. 3 The optimized structure of $CaCl_2$, CaOHCl, $CaCl_2\cdot H_2O$, non–planar $CaCl_2\cdot 2H_2O$, and planar $CaCl_2\cdot 2H_2O$. Bader charges (black, italic) and coordination lengths (in Å, blue) are shown. Color scheme: Ca = yellow, Cl = green, O = red, and H = white.

3.1.2 CaCl$_2$·2H$_2$O. Two stable conformers of CaCl$_2$·2H$_2$O are observed. The optimized non-planar structure of CaCl$_2$·2H$_2$O is shown in Fig. 3d and planar CaCl$_2$·2H$_2$O is shown in Fig. 3e. The planar symmetric structure does not form a H-bond between H and Cl atoms while its conformer (non-planar) does. The intra-molecular H-bonds provide extra stability of 4.78 kcal mol^{-1} to the non-planar structure (Fig. 3d) over the planar structure (Fig. 3e) and are responsible for the loss in symmetry of the non-planar molecule. The Bader charge on Cl differs by 0.04 in planar and non-planar structures due to the presence of a H-bond. The average Ca–O coordination length is the same (2.36 Å) in both of these structures, which is in good agreement with the Ca–O coordination length (2.32 Å) in the experimental crystalline structures.[31] There are two conformers reported for MgCl$_2$·2H$_2$O, which differ in energy by 4.53 kcal mol^{-1}.[15] Thus, H-bonds in CaCl$_2$·2H$_2$O provide 0.25 kcal mol^{-1} extra stability over MgCl$_2$·2H$_2$O.

3.1.3 CaCl$_2$·4H$_2$O. Calcium chloride tetrahydrate (CaCl$_2$·4H$_2$O) subsists into three crystalline structures.[32–34] We have chosen the initial structure of CaCl$_2$·4H$_2$O from these three crystalline phases and observed three stable structures shown in Fig. 4a–c. The optimized structure (ground state energy (U_{gr}) = −1628.66 kcal mol^{-1}) obtained from an α phase crystal has a slightly distorted octahedral geometry with four H-bonds. The average Ca–O coordination length is 2.42 Å, in good agreement with the α phase crystalline structure (2.42 Å).[32] The average Ca–Cl coordination length is 2.67 Å, in agreement with the α phase crystalline structure (2.8 Å).[32] The Bader charge on the Ca atom of the tetrahydrate (Fig. 4a) is 0.027 more positive than the Bader charge on the Ca atom of the dihydrate (Fig. 3d).

CaCl$_2$·4H$_2$O also exists in the β polymorph phase.[33] The initial molecular structure is chosen close to the β phase structure. The optimized structure is shown in Fig. 4b. The optimized geometry is a distorted octahedral with 1.62 kcal mol^{-1} more stable than the α phase optimized geometry (Fig. 4a). The average Ca–O coordination length in the β phase optimized gaseous tetrahydrate

is 2.405 Å, which is in agreement with the experimental β phase crystalline structure (2.46 Å).[33] Similarly, the average Ca–Cl coordination of the gaseous phase tetrahydrate is 2.68 Å, which is in close agreement with the β phase crystalline structure (2.74 Å).[33] There are two relatively strong H-bonds (OHCl) observed in the β phase optimized geometry compared to the α phase optimized geometry. There are intermolecular H-bonds (OHCl type) present in the β phase of the experimental crystalline structures,[33] while intramolecular H-bonds are observed in the gaseous molecule. This is the reason for the slight discrepancy in the structure of a gaseous molecule and the β phase crystalline structure.

CaCl$_2$·4H$_2$O also occurs in the γ phase.[34] The initial molecular structure is chosen close to the γ phase structure. The optimized structure is symmetrical and has almost a planar structure as shown in Fig. 4c. This structure is 19.24 kcal mol^{-1} less stable than the β phase optimized geometry. The average Ca–O coordination length is 2.26 Å in the γ phase optimized structure, which is in agreement with the γ phase crystalline structures (2.33 Å).[34] The two H atoms of surrounded H$_2$O molecules form a relatively strong H-bonds with the Cl compared to the α and the β phase optimized structures. The H$_2$O takes away the Cl atom from the Ca, hence the Ca–Cl distance becomes 4.06 Å. The Bader charge on Cl is 0.07 less electro-negative compared to the Cl of the β phase optimized structure. The Ca–Cl stretching and the lower atomic charge result in weaker electrostatic attraction between Ca–Cl pairs compared to α and β phase optimized structures. Thus, the γ optimized structure has lower stability over other conformers (α and β phase) despite having relatively strong H-bonds. The ∠Cl–H–O is 166.9°, which enables the greater availability of the Cl lone pairs for the anti-bonding Cl–H orbital overlap.

3.1.4 CaCl$_2$·6H$_2$O. We observe three stable gaseous structures of CaCl$_2$·6H$_2$O shown in Fig. 5a–c. The first conformer of the optimized CaCl$_2$·6H$_2$O (U_{gr} = −2319.15 kcal mol^{-1}) is shown in Fig. 5a. The average Ca–O coordination length is 2.86 Å and

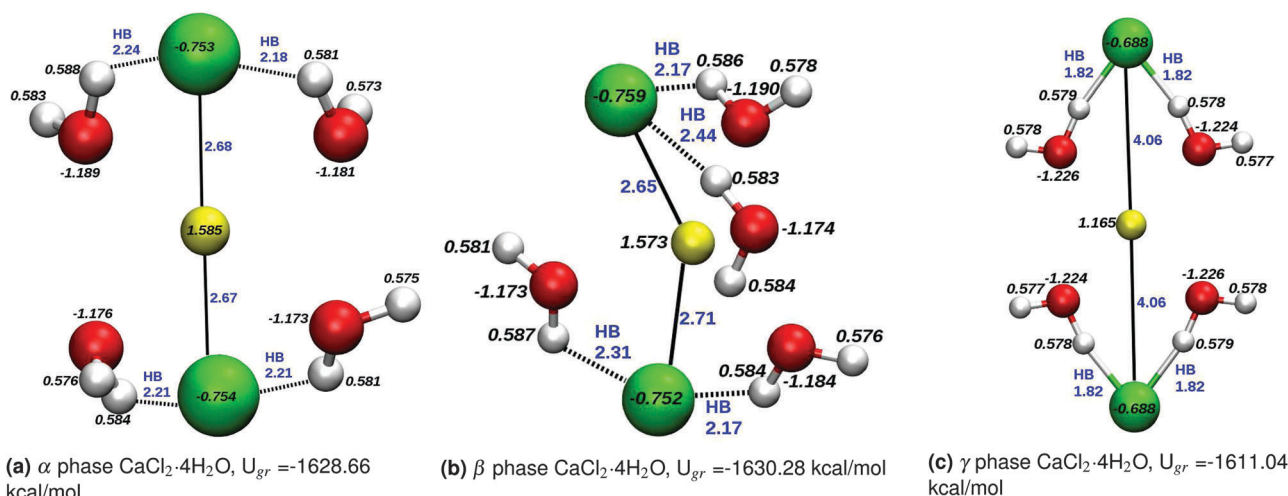**Fig. 4** The optimized structure of CaCl$_2$·4H$_2$O conformers. Bader charges (black, italic) and coordination lengths (in Å, blue) are shown. Color scheme: Ca = yellow, Cl = green, O = red, and H = white.
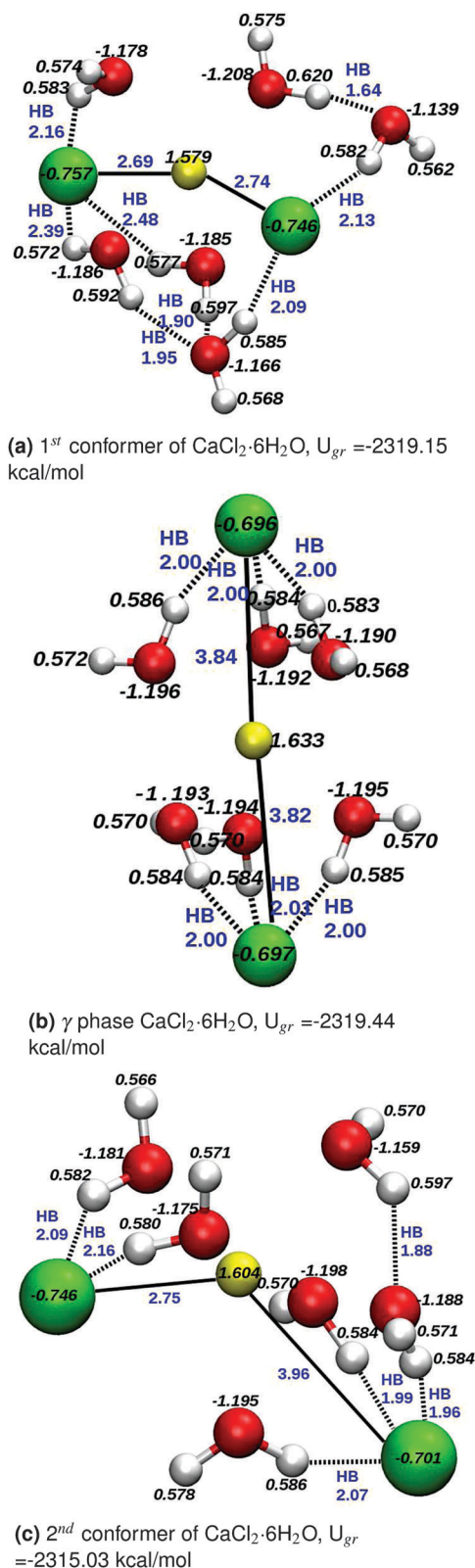
(a) α phase CaCl$_2$·4H$_2$O, U_{gr} = −1628.66 kcal/mol

(b) β phase CaCl$_2$·4H$_2$O, U_{gr} = −1630.28 kcal/mol

(c) γ phase CaCl$_2$·4H$_2$O, U_{gr} = −1611.04 kcal/mol

This journal is © the Owner Societies 2016

Phys. Chem. Chem. Phys., 2016, **18**, 10059–10069 | **10063**

(a) 1st conformer of CaCl$_2$·6H$_2$O, U_{gr} = −2319.15 kcal/mol

(b) γ phase CaCl$_2$·6H$_2$O, U_{gr} = −2319.44 kcal/mol

(c) 2nd conformer of CaCl$_2$·6H$_2$O, U_{gr} = −2315.03 kcal/mol

Fig. 5 The optimized structure of CaCl$_2$·6H$_2$O conformers. Bader charges (black, italic) and coordination lengths (in Å, blue) are shown. Color scheme: Ca = yellow, Cl = green, O = red, and H = white.

the average Ca–Cl coordination length is 2.72 Å. This optimized hexahydrate molecule (Fig. 5a) has four OHCl H-bonds (heteronuclear type) and three OHO H-bonds (homonuclear type). The average intramolecular H-bond length (2.19 Å) is in close agreement with the average intermolecular H-bond length (2.27 Å) present in the experimental γ phase crystalline structures.[35]

CaCl$_2$·6H$_2$O exists experimentally in the γ phase.[35] There are OHCl type intermolecular H-bonds present in the γ phase crystalline structures.[35] Those H-bonds are between the H of the H$_2$O of the hexahydrate and the Cl of the neighboring molecule of the hexahydrate in the crystal. The initial molecular structure is chosen close to the γ phase crystalline structure. In the optimized structure, the H$_2$O forms an octahedral with the Ca as shown in Fig. 5b. The optimized structure (Fig. 5b) forms six H-bonds (2.00 Å) of OHCl type. The average Ca–O coordination length of γ phase optimized CaCl$_2$·6H$_2$O is 2.37 Å. The average Ca–Cl coordination length is 3.84 Å. There is a discrepancy of 26.6% in the Ca–Cl coordination length of the gaseous hexahydrate and the γ phase crystalline hexahydrate. There are intramolecular H-bonds present in the gaseous γ phase of hexahydrate (Fig. 5b) while intermolecular H-bonds in the γ phase crystalline structures,[35] which explains the discrepancy.

The second stable conformer of the optimized CaCl$_2$·6H$_2$O is shown in Fig. 5c. This conformer is 4.12 kcal mol^{-1} less stable than the first conformer (Fig. 5a) and 4.41 kcal mol^{-1} less stable than the γ phase optimized structure (Fig. 5b). The average Ca–O coordination length is 2.45 Å. There are five intramolecular OHCl H-bonds (heteronuclear type) and one OHO type H-bond present in this conformer (Fig. 5c). Three H$_2$O molecules are forming H-bonds (OHCl type) with one Cl, one H$_2$O forms a H-bond (OHO type) with one of these H$_2$O molecules and two H$_2$O molecules form H-bonds with the other Cl atom. The average H···Cl H-bond length is 2.05 Å in the second stable conformer (Fig. 5c) while in the more stable γ phase optimized structure (Fig. 5b) it is 2.00 Å and 2.19 Å in the first conformer (Fig. 5a). The average O···H H-bond length is 1.88 Å in the second conformer (Fig. 5c) and in the first conformer, it is 1.83 Å. The O···H H-bonds are stronger in the first conformer, which explains the extra stability of the first conformer over the second conformer. The detailed explanation of H-bonds will be discussed in the section "Hydrogen bond in CaCl$_2$ hydrate system".

No conformer for MgCl$_2$·4H$_2$O and MgCl$_2$·6H$_2$O has been reported from DFT calculations.[15] To rationally compare the structure of CaCl$_2$ hydrates with MgCl$_2$ hydrates, the average Bader charge on each atom is compared in Table 1. The Bader charges on Ca and Cl atoms of CaCl$_2$ are lower in magnitude when compared with Mg and Cl in their analogous MgCl$_2$ hydrates. The Bader charge on Ca and Mg atoms increases monotonically with the hydration number. The magnitude of the Bader atomic charge on Cl in CaCl$_2$ hydrates decreases with hydration number whereas it increases from MgCl$_2$ to MgCl$_2$·2H$_2$O and decreases till MgCl$_2$·6H$_2$O. The magnitude of average Bader atomic charges on O and H in CaCl$_2$ hydrates is lower than MgCl$_2$ hydrates. The Ca–Cl, Ca–O distance in CaCl$_2$ hydrates is higher than MgCl$_2$ hydrates. Thus, electrostatic attractions

10064 | Phys. Chem. Chem. Phys., 2016, 18, 10059–10069

This journal is © the Owner Societies 2016

Table 1 Comparison of the Bader charge on various hydrates of $CaCl_2$ and $MgCl_2$[15] (only the lowest energy conformers are considered). An average charge is reported for many atoms of the same element in a molecule

Molecule	Ca (Mg)	Cl	O	H	Ca–O (Mg–O)	Ca–Cl (Mg–Cl)
$CaCl_2 \cdot 6H_2O$ ($MgCl_2 \cdot 6H_2O$)	1.633 (1.762)	−0.696 (−0.760)	−1.193 (−1.210)	0.577 (0.575)	2.37 (2.1)	3.83 (3.76)
$CaCl_2 \cdot 4H_2O$ ($MgCl_2 \cdot 4H_2O$)	1.573 (1.700)	−0.755 (−0.802)	−1.180 (−1.188)	0.582 (0.583)	2.40 (2.15)	2.68 (2.43)
$CaCl_2 \cdot 2H_2O$ ($MgCl_2 \cdot 2H_2O$)	1.558 (1.696)	−0.762 (−0.837)	−1.192 (−1.200)	0.587 (0.590)	2.36 (2.08)	2.54 (2.26)
$CaCl_2 \cdot H_2O$ ($MgCl_2 \cdot H_2O$)	1.554 (1.650)	−0.770 (−0.826)	−1.202 (−1.204)	0.594 (0.605)	2.33 (2.05)	2.49 (2.21)
$CaCl_2$ ($MgCl_2$)	1.553 (1.621)	−0.776 (−0.811)	N.A.	N.A.	N.A.	2.45 (2.18)

between Mg–O pairs in $MgCl_2$ hydrates are stronger than Ca–O pairs in $CaCl_2$ hydrates.

3.2 Reaction enthalpies of $CaCl_2$ hydrates

For reaction enthalpy calculations, we have considered the structure having minimum energy and no imaginary frequency. Table 2 describes the electronic ground state energy and various energy terms for all the studied hydrates. The binding energy ($\Delta E_{Binding}$) of a hydrate is defined as

$$\Delta E_{Binding} = E_{CaCl_2 \cdot nH_2O} - (E_{CaCl_2} + nE_{H_2O}) \qquad (13)$$

The enthalpy change during the dehydration reaction ($\Delta E_{Dehydration}$) is defined as

$$\Delta E_{Dehydration} = 0.5 \times [E_{CaCl_2 \cdot (n-2)H_2O} + 2E_{H_2O} - E_{CaCl_2 \cdot nH_2O}]$$
$$(n = 4, 6) \qquad (14)$$

$$\Delta E_{Dehydration} = [E_{CaCl_2 \cdot nH_2O} - E_{CaCl_2 \cdot (n-1)H_2O} - E_{H_2O}] \ (n = 1, 2) \qquad (15)$$

Similarly, the enthalpy change during the hydrolysis reaction ($\Delta E_{Hydrolysis}$) is defined as

$$\Delta E_{Hydrolysis} = [E_{CaOHCl} + (n - 1)E_{H_2O} + E_{HCl} - E_{CaCl_2 \cdot nH_2O}]$$
$$(n = 1, 2, 4, \& 6) \qquad (16)$$

The H_2O and HCl molecules are separately optimized using GGA-PW91 and TZ2P basis sets. The binding energy of $CaCl_2$ hydrates and their conformers depends on the Ca–Cl, Ca–O distance and on the strength of the intramolecular H-bond formed. The binding energy is the energy released on hydration per mole of salt, whereas the dehydration enthalpy is per mole of H_2O. For the monohydrate, the binding energy is the same as the enthalpy change in dehydration, but opposite in sign, and it is equal to −21.9 kcal mol^{-1}. The H_2O molecule attached with $CaCl_2$ forms a monohydrate. The attached H_2O forms a H-bond with the Cl of $CaCl_2$ (see Fig. 3c). Similarly, another H_2O molecule attached with the monohydrate and 20.48 kcal mol^{-1} energy is released. The strength of the H-bond in monohydrate

(2.24 Å, Fig. 3c) and in the dihydrate (2.205 Å, Fig. 3d) are of similar magnitude so the dehydration enthalpy is very close. The dehydration enthalpy released per H_2O molecule decreases from 21.9 kcal mol^{-1} to 14.56 kcal mol^{-1} for the increase in the hydration number from 1 to 6. The average negative atomic charge induced on the O of the H_2O molecule is decreased in magnitude from $CaCl_2 \cdot H_2O$ (−1.202) to $CaCl_2 \cdot 6H_2O$ (−1.184). This suggests that dehydration enthalpy is dominated by electrostatic attraction. The dehydration of two H_2O molecules from $CaCl_2 \cdot 6H_2O$ is easier than the removal of the two H_2O molecules from $CaCl_2 \cdot 4H_2O$ and so on. The enthalpy change in the hydrolysis reaction is very high for $CaCl_2 \cdot 6H_2O$ compared to the enthalpy change in dehydration as given in Table 2. The enthalpy change in hydrolysis decreases from higher hydrates to lower hydrates.

The enthalpy change during the dehydration and hydrolysis reaction of $CaCl_2$ hydrates is compared with $MgCl_2$ hydrates, as shown in Table 2. The dehydration enthalpy of $CaCl_2 \cdot 6H_2O$, $CaCl_2 \cdot 4H_2O$, and $CaCl_2 \cdot H_2O$ is slightly lower than analogous $MgCl_2$ hydrates. The dehydration enthalpy for $CaCl_2 \cdot 2H_2O$ is 26.8% higher than $MgCl_2 \cdot 2H_2O$, thus $CaCl_2 \cdot 2H_2O$ dehydrates at higher temperature compared with $MgCl_2 \cdot 2H_2O$. The $CaCl_2$ hydrates (except mono hydrate) have high enthalpy of hydrolysis compared to $MgCl_2$ hydrates (as given in Table 2) thus, $CaCl_2$ hydrates are more resistant to hydrolysis reaction.

3.3 Hydrogen bond in the $CaCl_2$ hydrate system

$CaCl_2$ hydrates have the OHCl type heteronuclear H-bond and the OHO type homonuclear H-bond. The strong H-bond has a predominant covalent character while the moderate H-bond has mostly electrostatic character.[38] The H-bond energy is a strong function of r_{X-H}, $r_{X\cdots H}$, and r_{X-Y} in XHX and XHY H-bonded systems.[39] The Cl atom is larger in size compared to O and less electronegative thus the availability of the lone pair for H-bond formation is lower compared to the O. Thus the OHO type H-bond is stronger than the OHCl type H-bond.[39]

In the present study, we observe the OHO type homonuclear H-bond in $CaCl_2 \cdot 6H_2O$ isomers (Fig. 5a and c). The strength of H-bonds depends on the distance between the donor H and the acceptor O distance (H-bond distance) and the $\angle O$–H$\cdots$O (H-bond angle). The $\angle O$–H$\cdots$O above 165° provides the complete lone pair availability in the O for the anti-bonding O–H orbital overlap[4,40] therefore stabilizing the H-bond. The non-bonded O$\cdots$H distance varies from 1.64 Å to 1.95 Å and $\angle O$–H$\cdots$O 135.92° to 165.48°. The lengthening of the O–H bond varies from 0.017 Å to 0.041 Å. These OHO type H-bonds are moderate in strength and predominantly electrostatic in nature.[38] In the first

Table 2 Energy of various hydrates and enthalpy change in dehydration and hydrolysis reactions (only the lowest energy conformers are considered). The parentheses value refers to analogous $MgCl_2$ hydrates[15]

Molecule	U_{gr}/kcal mol^{-1}	$\Delta E_{Binding}$/ kcal mol^{-1}	$\Delta E_{Dehydration}$/ kcal mol^{-1}	$\Delta E_{Hydrolysis}$/ kcal mol^{-1}
$CaCl_2 \cdot 6H_2O$	−2319.15	−104.65	14.56 (14.8)	121.68 (119.3)
$CaCl_2 \cdot 4H_2O$	−1630.28	−75.52	16.57 (16.7)	92.55 (89.7)
$CaCl_2 \cdot 2H_2O$	−937.40	−42.38	21.19 (15.7)	59.41 (46.3)
$CaCl_2 \cdot H_2O$	−587.05	−21.9	21.9 (22.4)	38.93 (40.3)

conformer of $CaCl_2·6H_2O$ (Fig. 5a), three H-bonds of this type are present while in the second conformer of $CaCl_2·6H_2O$ (Fig. 5c) only one H-bond is present. The first conformer of $CaCl_2·6H_2O$ has one relatively strong but moderate strength H-bond (1.64 Å) thus provides 4.12 kcal mol^{-1} stability over the second conformer.

The $CaCl_2$ hydrates have mostly OHCl type heteronuclear H-bonds. The H atoms of the hydrated $CaCl_2·XH_2O$ molecule are attracted by adjacent Cl atoms and form OHCl type H bonds. In the present case, the $Cl\cdots H$ distance varies from 1.82 Å to 2.48 Å and the Cl–O distance varies from 2.86 Å to 3.15 Å. The lengthening of the OH bond varies from 0.01 Å to 0.08 Å. A similar bond length of H-bonds is observed in organic and organometallic crystals.[41] Tommaso et al. also observed the OHCl type H-bond in the hydration of Ca^{2+} ions in salt solution.[18] The bond valence is proportional to the electron density. The bond valence of the atom is distributed between the bonds which it forms. Each bond involves the same number of electrons. The BV sum rule is described as

$$S_{H-O} + S_{H\cdots Cl} = 1 \qquad (17)$$

In heteronuclear H-bonds, the BV sum rule (eqn (17)) has four parameters (two of O–H and two of $H\cdots Cl$). From Fig. 6, it is evident that heteronuclear H-bonds follow the BV sum rule in close agreement ($R^2 = 0.98$). Therefore, the BV sum rule is applicable for this class of H-bonds. The bond parameters R_0 and b for $H\cdots Cl$ are 0.96 Å, 0.80 Å and for the H–O pair 0.97 Å, 0.38 Å, which is in agreement with the literature.[4,25] The strength of the H-bond is inversely related to the $H\cdots Cl$ distance. The non-bonded $H\cdots Cl$ distance depends on $\angle O$–$H\cdots Cl$, which varies from 166.9° to 123° in $CaCl_2$ hydrates. The larger $\angle O$–$H\cdots Cl$ ($>165°$) facilitates anti-bonding $Cl\cdots H$ orbital overlap and favors hydrogen bonding. Most of these ($\sim 77\%$) OHCl type H-bonds are moderate and weak in strength and are dominated by electrostatic interactions and dispersion.[38] In $CaCl_2·4H_2O$, the H-bonds destabilize the structure by 19.24 kcal mol^{-1} while stabilize the $CaCl_2·6H_2O$ and $CaCl_2·2H_2O$ by 4.41 kcal mol^{-1} and 4.78 kcal mol^{-1} respectively. This suggests that the formation of strong H-bonds

in $CaCl_2·4H_2O$ could form metastable states and may result in sluggish hydration kinetics.

3.4 Equilibrium product concentrations

The ΔG of a system is a function of pressure, temperature, and the system characteristics. At chemical equilibrium, the ΔG (from eqn (7)) should be zero and this will provide information about the equilibrium concentration of products.

3.4.1 Dehydration reaction of $CaCl_2$ hydrates and their comparison with $MgCl_2$ hydrates. In the dehydration reaction, the higher hydrate absorbs energy and disintegrates into lower hydrates and H_2O molecules. In the experimental dehydration set-up only the water vapor pressure (p_{H_2O}) and the HCl pressure (p_{HCl}) are the controlled variables. The partial pressure (concentration) of hydrates is not important. In the present study, the partial pressure of water and system temperature are the control variables, while the partial pressure of hydrates is kept constant at 1 atm. The equilibrium water vapor pressure depends on the system temperature for all dehydration reactions of both hydrates ($CaCl_2$ and $MgCl_2$) as shown in Fig. 7. It is recognizable from Fig. 7 that dehydration from hexahydrate to tetrahydrate is easier (favored at lower temperature) than from tetra to dihydrate and from dihydrate to monohydrate for $CaCl_2$ and $MgCl_2$ hydrates. This trend of dehydration of various $CaCl_2$ hydrates is similar to the experimental results[9,10] and outlined as well by the enthalpy of dehydration in Table 2, where the enthalpy of dehydration increases from hexa to monohydrate.

Rammelberg et al.[10] reported from thermal gravimetric analysis/differential scanning calorimetry (TGA/DSC) measurements 30% conversion of $CaCl_2·6H_2O$ to $CaCl_2·4H_2O$ at 336 K. In the present study, we observed 30% conversion of $CaCl_2·6H_2O$ to $CaCl_2·4H_2O$ only at around 340 K. There is an offset of 4 K is observed. The effect of temperature on the equilibrium dehydration curve of $CaCl_2·6H_2O$ (slope = 0.035) is in agreement with the experiments (slope = 0.032)[9,42] as shown in Fig. 7. An offset of 20 K is observed in the low vapor regime (<0.03 atm) for $CaCl_2·6H_2O$. The offset may be a consequence of the ideal polyatomic gas phase assumption. Another reason could be that the equilibrium product concentrations obtained from ΔG (DFT calculations) reports the static equilibrium properties while the experimental (TGA/DSC)
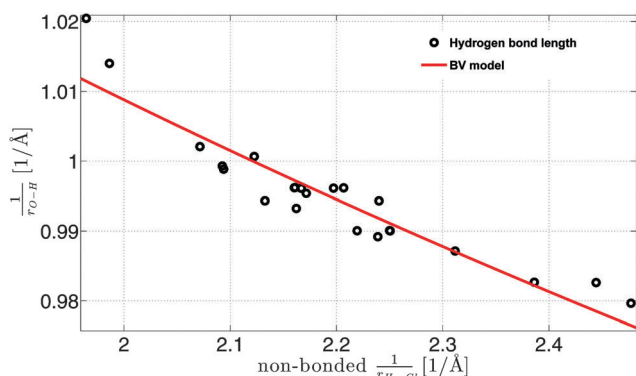

Fig. 6 Correlation of $H\cdots Cl$ bond length (non-bonded interaction) with OH bond length of surrounding H_2O in all the hydrates of $CaCl_2$. The non-bonded $Cl\cdots H$ distance versus OH bond length obeys the BV sum rule, which is shown as a continuous curve.
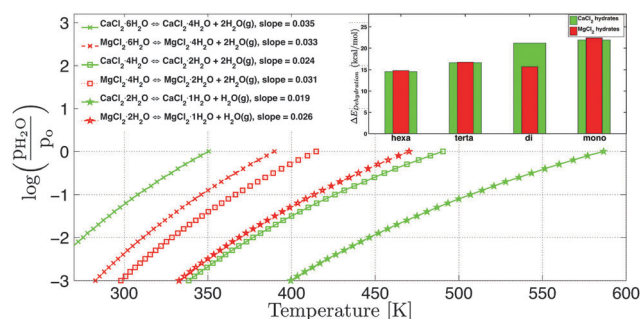

Fig. 7 Equilibrium vapor pressure for the dehydration reactions of $CaCl_2$ hydrates (green) at various temperatures and constant partial pressure of hydrate, $p_0 = 1$ atm. The dashed red lines represent the dehydration curves of $MgCl_2$ hydrates.[15] The inset graph shows the comparison of enthalpy change during the dehydration reactions of $CaCl_2$ and $MgCl_2$ hydrates.

10066 | Phys. Chem. Chem. Phys., 2016, 18, 10059–10069

This journal is © the Owner Societies 2016

kinetics reports the dynamic equilibrium properties. There is a similar offset observed in the equilibrium dehydration curve for $CaCl_2 \cdot 4H_2O$ to $CaCl_2 \cdot 2H_2O$ as well. The equilibrium partial vapor pressure (p_{H_2O}) of 1 atm is observed at 350.5 K for $CaCl_2 \cdot 6H_2O$ while at 490.5 K and 586.5 K for $CaCl_2 \cdot 4H_2O$ and $CaCl_2 \cdot 2H_2O$ as shown in Fig. 7.

The gradient of the dehydration curve for $CaCl_2 \cdot 6H_2O$ is 0.002 higher than $MgCl_2 \cdot 6H_2O$ while 0.007 lower for $CaCl_2 \cdot 4H_2O$ and $CaCl_2 \cdot 2H_2O$ when compared with their analogous $MgCl_2$ hydrates. Thus, $CaCl_2 \cdot 6H_2O$ has the shortest range of dehydration temperature while $CaCl_2 \cdot 4H_2O$ and $CaCl_2 \cdot 2H_2O$ have a higher temperature range of operation. The dehydration enthalpy of $CaCl_2 \cdot 6H_2O$ is 0.25 kcal mol^{-1} lower than $MgCl_2 \cdot 6H_2O$ (as given in Table 2) thus it dehydrates at lower temperature compared to $MgCl_2 \cdot 6H_2O$. The dehydration enthalpy of $CaCl_2 \cdot 4H_2O$ is 0.13 kcal mol^{-1} lower than $MgCl_2 \cdot 4H_2O$ while $CaCl_2 \cdot 4H_2O$ dehydrates at higher temperature than $MgCl_2 \cdot 4H_2O$. This behavior can be explained from the role of the meta-stable conformer formed due to presence of strong H-bonds present in the $CaCl_2 \cdot 4H_2O$ isomer (Fig. 4c). The dehydration enthalpy of $CaCl_2 \cdot 2H_2O$ is 5.3 kcal mol^{-1} higher than $MgCl_2 \cdot 2H_2O$ (see inset graph of Fig. 7) so it dehydrates at higher temperature compared with $MgCl_2 \cdot 2H_2O$.

3.4.2 Hydrolysis reaction of $CaCl_2$ hydrates and their comparison with $MgCl_2$ hydrates.

In the hydrolysis reaction, higher hydrates disintegrate into $CaOHCl/MgOHCl$, H_2O, and HCl. We have chosen an arbitrary low HCl partial pressure ($p_{HCl} = 1 \times 10^{-3}$ atm) as a safety limit. The low equilibrium partial pressure of HCl ($p_{HCl} = 1 \times 10^{-3}$ atm) will result in a low driving force for the hydrolysis reaction and a slow down in the hydrolysis kinetics. Hydrolysis reactions can affect the cycle stability of $MgCl_2/CaCl_2$ hydrates. To understand the effect of H_2O partial pressure (p_{H_2O}) at fixed HCl partial pressures ($p_{HCl} = 1 \times 10^{-3}$ atm) on the hydrolysis of $CaCl_2$ hydrates and $MgCl_2$ hydrates, equilibrium H_2O vapor pressure (p_{H_2O}) and hydrolysis temperature are plotted in Fig. 8. The difference between Fig. 7 and 8 is that in the latter case, hydrolysis is considered under constant HCl partial pressure ($p_{HCl} = 1 \times 10^{-3}$ atm).
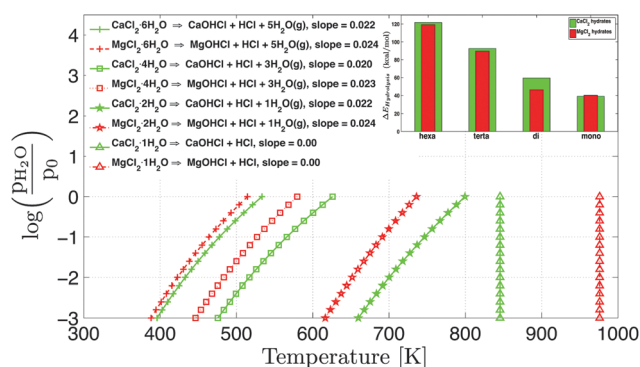

Fig. 8 Equilibrium vapor pressure for the hydrolysis reactions of $CaCl_2$ hydrates (green) at various temperatures and fixed HCl pressure $p_{HCl} = 1 \times 10^{-3}$ atm and $p_0 = 1$ atm. The dashed red lines represent the hydrolysis curves of $MgCl_2$ hydrates.[15] The inset graph shows the comparison of enthalpy change during the hydrolysis reactions of $CaCl_2$ and $MgCl_2$ hydrates.

Hydrolysis starts at higher temperature (>396 K) in comparison to dehydration for all the hydrates of $CaCl_2$, which is consistent with the enthalpy change in hydrolysis (38.93 kcal mol^{-1} to 121.68 kcal mol^{-1}) and dehydration (21.9 kcal mol^{-1} to 14.56 kcal mol^{-1}) as given in Table 2.

The equilibrium vapor pressure of 1 atm is observed from $CaCl_2 \cdot 6H_2O$ at 350.5 K and hydrolysis above the safety limit ($p_{HCl} = 1 \times 10^{-3}$ atm) starts at 396 K. There is no overlapping temperature region between hydrolysis and dehydration for $CaCl_2 \cdot 6H_2O$. The $CaCl_2 \cdot 4H_2O$ dehydrates into $CaCl_2 \cdot 2H_2O$ at 490.5 K ($p_{H_2O} = 1$ atm) while hydrolysis starts (above safety limit, $p_{HCl} > 1 \times 10^{-3}$ atm) at 475.8 K. There is an overlap of around 14.7 K (from Fig. 7 and 8). Similarly the overlap for the $CaCl_2 \cdot 2H_2O$ is around 32.5 K. Fraissler et al.[14] reported experimentally from TGA measurements that the HCl formation from thermal decomposition of $CaCl_2$ salt hydrates occurs in the temperature range of 683–1013 K. We observe the starting point ($p_{HCl} = 1 \times 10^{-3}$ atm, onset) of HCl formation for $CaCl_2 \cdot 2H_2O$ and $CaCl_2 \cdot H_2O$ at 660 K and 845 K ($p_{H_2O} = 1 \times 10^{-3}$ atm) respectively. $CaCl_2 \cdot 4H_2O$ and $CaCl_2 \cdot 6H_2O$ will not be present in this temperature range. The offset in the onset of HCl formation temperature may be the consequence of the dynamic and static equilibrium comparison and the effect of the ideal polyatomic gas assumption. The hydrolysis of $CaCl_2 \cdot H_2O$ is independent of the H_2O vapor pressure as shown in Fig. 8.

Hydrolysis of $MgCl_2$ hydrates starts at lower temperature in comparison to $CaCl_2$ hydrates for hexa, tetra, and dihydrates, which is consistent with the enthalpy change in hydrolysis of $MgCl_2$ and $CaCl_2$ hydrates as given in Table 2. The slope of the $MgCl_2$ hydrate hydrolysis curve is slightly higher compared to the $CaCl_2$ hydrates so the hydrolysis of $CaCl_2$ hydrates has a longer operating temperature range. Hydrolysis in $MgCl_2 \cdot 6H_2O$, $MgCl_2 \cdot 4H_2O$ and $MgCl_2 \cdot 2H_2O$ starts at 388, 446, and 616 K ($p_{H_2O} = 1 \times 10^{-3}$ atm) respectively, which is lower than analogous $CaCl_2$ hydrates. Hydrolysis in $CaCl_2 \cdot H_2O$ starts at lower temperature (845 K) than $MgCl_2 \cdot H_2O$ (976 K). Thus, $CaCl_2$ hydrates have improved hydrolysis resistance if the operating temperature is less than 800 K.

Furthermore, the partial pressure of HCl (p_{HCl}) is plotted with their equilibrium temperature at fixed H_2O vapor pressure ($p_{H_2O} = 4 \times 10^{-3}$ atm) for $MgCl_2$ and $CaCl_2$ hydrates in Fig. 9. For any temperature (<761 K), $MgCl_2$ will always have high partial pressure of HCl (p_{HCl}) compared to $CaCl_2$ hydrates. The slope of the equilibrium hydrolysis curve (Fig. 9) decreases from the hexahydrate to the monohydrate for both $CaCl_2$ and $MgCl_2$ hydrates. The slope of $CaCl_2$ is slightly lower than analogous $MgCl_2$ hydrates. Hence, the HCl concentration could be better controlled with temperature in $CaCl_2$ hydrates over $MgCl_2$ hydrates.

For a given change in partial pressure of HCl (p_{HCl}), the temperature changes maximum for the monohydrate. The reason for the change in the slope of the hydrolysis curve can be explained by the stoichiometric ratio between HCl and H_2O. The stoichiometric ratio of HCl to H_2O increases from 0.2 to 1 for the hexahydrate to the monohydrate. Thus, the molar ratio between HCl and H_2O decreases from mono to hexahydrate, therefore, temperature varies maximum for the monohydrate for a given change in p_{HCl}. The similar trend of slope is observed for $MgCl_2$ hydrates.
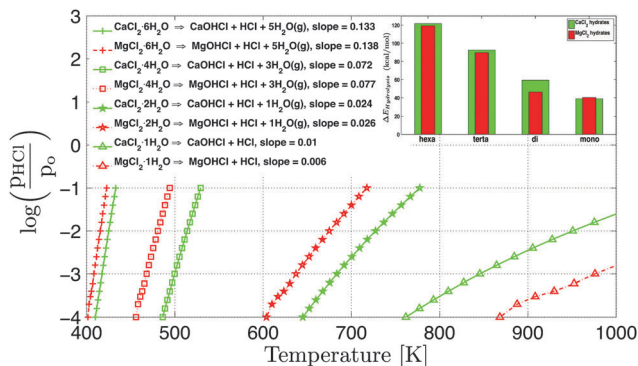
This journal is © the Owner Societies 2016

Phys. Chem. Chem. Phys., 2016, 18, 10059–10069 | 10067

Fig. 9 Equilibrium vapor pressure for the hydrolysis reactions of $CaCl_2$ hydrates (green) at various temperatures and fixed H_2O pressure $p_{H_2O} = 4 \times 10^{-3}$ atm and $p_0 = 1$ atm. The dashed red lines represent the hydrolysis curves of $MgCl_2$ hydrates.[15] The inset graph shows the comparison of enthalpy change during the hydrolysis reactions of $CaCl_2$ and $MgCl_2$ hydrates.
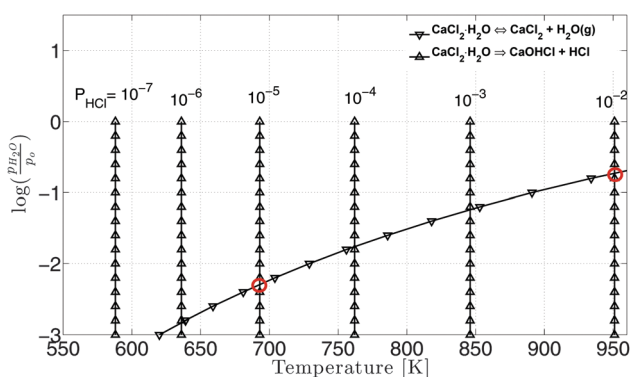

Fig. 10 Equilibrium water vapor pressure for hydrolysis and dehydration reactions at different temperatures. p_{HCl} is varied from 10^{-7} to 10^{-2} atm and $p_0 = 1$ atm.

3.4.3 Preferential hydrolysis over dehydration for $CaCl_2 \cdot H_2O$. The hydrolysis of $CaCl_2 \cdot H_2O$ is different from the hydrolysis of higher hydrates as H_2O is not produced in this reaction. Dehydration and hydrolysis reaction compete with each other at higher temperature for $CaCl_2 \cdot H_2O$. Fig. 10 shows the equilibrium curve for dehydration and hydrolysis for $CaCl_2 \cdot H_2O$ at different HCl partial pressure and H_2O pressure. It is evident that equilibrium temperature decreases with a decrease in partial pressure of HCl, while hydrolysis becomes thermodynamically favorable over dehydration at low partial pressure of HCl. The equilibrium water vapor pressure (p_{H_2O}) and temperature at the low HCl partial pressure (1×10^{-5} atm) are 4×10^{-3} atm and 693 K. The equilibrium water vapor pressure (p_{H_2O}) and temperature increase with an increase in the HCl partial pressure. The equilibrium p_{H_2O} and temperature become 0.16 atm and 950 K at the high HCl partial pressure $p_{HCl} = 1 \times 10^{-2}$ atm.

4 Conclusions

To understand the equilibrium product concentrations of the dehydration and hydrolysis reactions of $CaCl_2 \cdot nH_2O$ in comparison to $MgCl_2 \cdot nH_2O$, DFT calculations have been carried out.

The structural properties of $CaCl_2$ hydrates along with their atomic charges are analyzed. This study reveals the formation of many conformers due to the presence of various H-bonds. The relative stability of a conformer and dehydration enthalpy is dominated by electrostatic attraction and strength of H-bond formed. We observed a homonuclear H-bond (OHO) and a heteronuclear H-bond (OHCl) in the various hydrates of $CaCl_2$. Most of the H-bonds ($\sim 77\%$) in $CaCl_2$ hydrate are of moderate strength. $CaCl_2 \cdot 2H_2O$ has two conformers due to the presence of an OHCl type H-bond. Similarly, three conformers of $CaCl_2 \cdot 4H_2O$, and $CaCl_2 \cdot 6H_2O$ are observed. The most stable conformers are non-planar $CaCl_2 \cdot 2H_2O$ (Fig. 3d), β phase optimized $CaCl_2 \cdot 4H_2O$ (Fig. 4b), and γ phase optimized $CaCl_2 \cdot 6H_2O$ (Fig. 5b). These conformers are 4.78, 19.24, and 4.41 kcal mol^{-1} more stable than their lowest stable conformer. The relatively strong OHCl H-bonds provide 4.41 kcal mol^{-1} stability compared to its lowest stable conformer in $CaCl_2 \cdot 6H_2O$. The H-bonds in $CaCl_2 \cdot 4H_2O$ destabilize the γ phase optimized structure by 19.24 kcal mol^{-1} compared with the β phase optimized structure. This implies that $CaCl_2 \cdot 4H_2O$ could form a metastable stage, and may have a sluggish hydration kinetics. Both $CaCl_2 \cdot 2H_2O$ and $CaCl_2 \cdot 6H_2O$ have less stable conformers, consequently they do not form metastable stages. Thus, the H-bonds should not markedly affect their hydration kinetics. The BV sum rule parameters for OHCl type H-bonds are 0.96 Å, 0.80 Å (for H⋯Cl pair) and 0.97 Å, 0.38 Å (for H⋯O pair). These parameters can be used to characterize the OHCl H-bonded system.

The enthalpy change in the dehydration and hydrolysis reactions of $CaCl_2$ hydrates is obtained from DFT and compared with $MgCl_2$ hydrates. The equilibrium composition of dehydration and hydrolysis reactions is obtained by equating the ΔG to zero over a wide range of temperature and pressure conditions. The trend in the dehydration reaction is similar to the experiments for all the $CaCl_2$ hydrates. The effect of temperature on the dehydration of $CaCl_2 \cdot 6H_2O$ (slope = 0.035) is in close agreement with experiments (slope = 0.032).[9,10] We compared the equilibrium composition of dehydration and hydrolysis reactions for $CaCl_2$ and $MgCl_2$ hydrates. The $CaCl_2 \cdot 6H_2O$ dehydrates at lower temperature (as shown in Fig. 7) compared with $MgCl_2 \cdot 6H_2O$ while $CaCl_2 \cdot 4H_2O$ and $CaCl_2 \cdot 2H_2O$ dehydrates at higher temperature when compared to their analogous $MgCl_2$ hydrates. The $CaCl_2$ hydrates have better temperature control with the partial pressure of the products (p_{HCl}, p_{H_2O}) when compared to the $MgCl_2$ hydrates. We investigated hydrolysis and dehydration at different temperature, pressure regimes for $CaCl_2$ and $MgCl_2$ hydrates. The $CaCl_2$ hydrates have better hydrolysis resistance over $MgCl_2$ hydrates in the temperature range 273 to 800 K, which explains the higher stability in the mixture of $CaCl_2$ and $MgCl_2$ hydrates. Hydrolysis is very rare for $CaCl_2 \cdot 6H_2O$ because the onset of hydrolysis reaction at the safety limit ($p_{HCl} = 1 \times 10^{-3}$ atm) is higher than the dehydration temperature of $CaCl_2 \cdot 6H_2O$. Similarly $CaCl_2 \cdot 4H_2O$ and $CaCl_2 \cdot 2H_2O$ can undergo hydrolysis ($p_{HCl} = 1 \times 10^{-3}$ atm) at 475.8 and 660 K respectively. The similar temperatures for $MgCl_2$ hydrates are 446 and 616 K. $CaCl_2 \cdot H_2O$ may undergo hydrolysis above 850 K. These temperature ranges should be

10068 | *Phys. Chem. Chem. Phys.,* 2016, **18**, 10059–10069

This journal is © the Owner Societies 2016

treated as the safety limit range for hydrolysis reactions. The CaCl$_2$ hydrates could be mixed with MgCl$_2$ hydrates to improve the hydrolysis resistance and therefore durability of the system.

Acknowledgements

References

1 A. Sharma, V. Tyagi, C. Chen and D. Buddhi, *Renewable Sustainable Energy Rev.*, 2009, **13**, 318–345.

2 K. E. N'Tsoukpoe, H. Liu, N. Le Pierrès and L. Luo, *Renewable Sustainable Energy Rev.*, 2009, **13**, 2385–2396.

3 K. E. N'Tsoukpoe, T. Schmidt, H. U. Rammelberg, B. A. Watts and W. K. Ruck, *Appl. Energy*, 2014, **124**, 1–16.

4 E. Iype, S. V. Nedea, C. C. M. Rindt, A. A. van Steenhoven, H. A. Zondag and A. P. J. Jansen, *J. Phys. Chem. C*, 2012, **116**, 18584–18590.

5 Y. Kirsh, S. Yariv and S. Shoval, *J. Therm. Anal.*, 1987, **32**, 393–408.

6 S. Shoval, S. Yariv, Y. Kirsh and H. Peled, *Thermochim. Acta*, 1986, **109**, 207–226.

7 H. U. Rammelberg, M. Myrau, T. Schmidt and W. Ruck, *IMPRES 2013, Fukuoka, 04.-06*, 2013.

8 F. Trausel, A.-J. de Jong and R. Cuypers, *Energy Procedia*, 2014, **48**, 447–452.

9 H. Zondag, M. van Essen, L. Bleijendaal, J. Cot, R. Schuitema, W. van Helden, W. Planje, T. Epema and H. Oversloot, *Proceeding of IRES*, 2008.

10 H. U. Rammelberg, T. Schmidt and W. Ruck, *Energy Procedia*, 2012, **30**, 362–369.

11 C. C. Wilkins, N. W. Hunter and E. F. Pearson, *J. Chem. Educ.*, 1992, **69**, 753.

12 K. E. N'Tsoukpoe, H. U. Rammelberg, A. F. Lele, K. Korhammer, B. A. Watts, T. Schmidt and W. K. Ruck, *Appl. Therm. Eng.*, 2015, **75**, 513–531.

13 A. Krönauer, E. Lävemann, S. Brückner and A. Hauer, *Energy Procedia*, 2015, **73**, 272–280.

14 G. Fraissler, M. Jöller, T. Brunner and I. Obernberger, *Chem. Eng. Process.*, 2009, **48**, 380–388.

15 B. Smeets, E. Iype, S. V. Nedea, H. A. Zondag and C. C. M. Rindt, *J. Chem. Phys.*, 2013, **139**, 124312.

16 C. M. Widdifield and D. L. Bryce, *Can. J. Chem.*, 2011, **89**, 754–763.

17 C. M. Widdifield, I. Moudrakovski and D. L. Bryce, *Phys. Chem. Chem. Phys.*, 2014, **16**, 13340–13359.

18 D. Di Tommaso, E. Ruiz-Agudo, N. H. de Leeuw, A. Putnis and C. V. Putnis, *Phys. Chem. Chem. Phys.*, 2014, **16**, 7772–7785.

19 M. Pavlov, P. E. Siegbahn and M. Sandström, *J. Phys. Chem. A*, 1998, **102**, 219–228.

20 X. Lei and B. Pan, *J. Phys. Chem. A*, 2010, **114**, 7595–7603.

21 T. Todorova, P. H. Hünenberger and J. Hutter, *J. Chem. Theory Comput.*, 2008, **4**, 779–789.

22 M. Peschke, A. T. Blades and P. Kebarle, *J. Phys. Chem. A*, 1998, **102**, 9978–9985.

23 A. A. Zavitsas, *J. Phys. Chem. B*, 2005, **109**, 20636–20640.

24 S. Lan, H. Zondag, A. van Steenhoven and C. Rindt, *J. Therm. Anal. Calorim.*, 2016, 1–10.

25 I. D. Brown, *Chem. Rev.*, 2009, **109**, 6858–6919.

26 L. Sobczyk, S. J. Grabowski and T. M. Krygowski, *Chem. Rev.*, 2005, **105**, 3513–3560.

27 J. P. Perdew, J. Chevary, S. Vosko, K. A. Jackson, M. R. Pederson, D. Singh and C. Fiolhais, *Phys. Rev. B: Condens. Matter Mater. Phys.*, 1992, **46**, 6671–6687.

28 G. Te Velde, F. M. Bickelhaupt, E. J. Baerends, C. Fonseca Guerra, S. J. A. van Gisbergen, J. G. Snijders and T. Ziegler, *J. Comput. Chem.*, 2001, **22**, 931–967.

29 M. M. Probst, T. Radnai, K. Heinzinger, P. Bopp and B. M. Rode, *J. Phys. Chem.*, 1985, **89**, 753–759.

30 D. A. McQuarrie, *Statistical mechanics*, Harper & Row, 1975.

31 A. Leclaire and M. M. Borel, *Acta Crystallogr., Sect. B: Struct. Crystallogr. Cryst. Chem.*, 1977, **33**, 1608–1610.

32 A. Leclaire and M. Borel, *Acta Crystallogr., Sect. B: Struct. Crystallogr. Cryst. Chem.*, 1979, **35**, 585–588.

33 A. Leclaire and M. Borel, *Acta Crystallogr., Sect. B: Struct. Crystallogr. Cryst. Chem.*, 1978, **34**, 902–904.

34 A. Leclaire, M. Borel and J. Monier, *Acta Crystallogr., Sect. B: Struct. Crystallogr. Cryst. Chem.*, 1980, **36**, 2757–2759.

35 P. A. Agron and W. R. Busing, *Acta Crystallogr., Sect. C: Cryst. Struct. Commun.*, 1986, **42**, 141–143.

36 P. F. Weck and E. Kim, *J. Phys. Chem. C*, 2014, **118**, 4618–4625.

37 R. W. G. Wyckoff, *Crystal Structures*, 1963, vol. 1, pp. 239–444.

38 S. Grabowski, *Hydrogen Bonding – New Insights*, Springer Netherlands, 2006.

39 P. A. Kollman and L. C. Allen, *Chem. Rev.*, 1972, **72**, 283–303.

40 P. Gilli, V. Bertolasi, V. Ferretti and G. Gilli, *J. Am. Chem. Soc.*, 1994, **116**, 909–915.

41 T. Steiner, *J. Phys. Chem. A*, 1998, **102**, 7041–7052.

42 http://www.prog-univers.com/IMG/pdf/CalciumChloridHandbook-2.pdf.

This journal is © the Owner Societies 2016

Phys. Chem. Chem. Phys., 2016, **18**, 10059–10069 | **10069**